



Thermal Spray Coatings for Erosion–Corrosion Resistant Applications

P. Suresh Babu¹  · Y. Madhavi¹ · L. Rama Krishna¹ · G. Sivakumar¹ · D. Srinivasa Rao¹ · G. Padmanabham¹

Received: 5 May 2020 / Accepted: 26 July 2020 / Published online: 10 August 2020
© The Indian Institute of Metals - IIM 2020

Abstract Thermal spray techniques have been extensively used to deposit coatings of varying compositions on a variety of industrial components for life enhancement under wear and corrosion prone environments at ambient and high temperatures. A number of components used in power generation systems most commonly encounter high-temperature erosion–corrosion. This review article briefly summarizes various thermal spray techniques and coating characteristics that are relevant to erosion–corrosion applications followed by detailed discussion on the erosion–corrosion fundamentals and testing methods. Further, ambient and high-temperature erosion–corrosion behavior of WC- and CrC-based cermet coatings and oxide coatings have been investigated, compared, analyzed and presented. Based on the analysis of results reported so far, the methodologies to enhance the erosion–corrosion resistance of coatings have been proposed both for ambient and high temperature applications. The future scope of work that needs to be explored to contribute further developments has also been identified and presented.

Keywords Thermal spray · Erosion–corrosion · Oxidation · HVOF · Plasma spray · Detonation spray

1 Introduction

The industrial components such as pipes used for transporting the petrochemical products, superheater tubes and re-heater tubes, heat exchangers, propellers, impellers, orifices and turbine blades in power generation are susceptible to erosion–corrosion damage, especially because they encounter suspended particles in the corrosive gaseous or liquid medium [1–3]. In erosion, the material loss is purely by mechanical action generated by the suspended particles impacting the surface of a component. For instance, the material removal mechanism associated with sand or grit blasting is the simplistic example to understand the erosion process [4, 5], whereas in the erosion–corrosion process, the surface undergoes a chemical change due to interaction with the corrosive environment and the corrosion product may eventually get detached from its location due to mechanical action of impinged particles [6–8]. Therefore, in the presence of corrosion medium, the overall material loss due to combined erosion and corrosion will be higher than the material loss due to erosion alone.

Nevertheless, the total wear loss of material depends on the environmental conditions, where the oxide layer formed on the material surface acts as a protective layer and may sometimes reduce the overall loss [9, 10]. However, the erosion–corrosion mechanisms are not completely understood due to complexity involved in material loss due to synergetic action of corrosion on erosion and vice versa. At the same time, it is also interesting to note that the metal ions that are formed due to corrosion are swept away by the surrounding fluid flow before a well-defined corrosion product is formed, thus contributing to the additional complications in understanding the mechanistic aspects of surface damage.

✉ P. Suresh Babu
pitchuka@arci.res.in;
http://arci.res.in/

¹ International Advanced Research Centre for Powder Metallurgy and New Materials (ARCI), Balapur (P.O), Hyderabad 500005, India

It is to be noted that the critical components that are subjected to severe wear conditions demand their frequent replacement affecting the operational continuity. Therefore, the efficiency of protective coatings to extend the service life of components in the power generation systems has been explored worldwide [11]. The typical environment in power generation system that includes corrosive chloride/sulfate gases assisted by the prevailed high temperature drives the continuous degradation of critical components. Further, the fly ash generated in the coal-fired boilers resulting in an eventual component damage has been a long-standing aspect that needs focused attention of both design engineers and operational teams [12–15]. Similarly, efforts have been made in petrochemical industries to enhance the service life of various components subjected to erosion–corrosion by deploying the coated components. In order to enhance the life of such components, the chosen coating is expected to act as a barrier between component surface and damage-prone surrounding environment [16, 17].

Towards catering the solutions for such industrial requirements, many coating materials as well as coating technologies and their combinations have been attempted extensively during the last two decades [10, 18]. Among various coating deposition methods such as thermal spray, electrodeposition, vapor deposition and laser deposition, the thermal spray processes are widely accepted by aerospace, power generation, textile, automotive, petrochemical and other industries. The technological advantages, namely the high productivity (deposition rate), flexibility to deposit a wide range of materials, availability of well-automated and portable spray systems together with the ability to refurbish the damaged components through localized repairs, make the thermal spray as a most preferred alternative than the other techniques [11]. In the context that the deployment of thermally sprayed coatings to combat erosion–corrosion and erosion–oxidation has been constantly increasing, the present review article is expected to provide a leap momentum to comprehensively understand this interesting field and therefore drives the focused industrial adaptability [10].

An analysis of the literature indicates the availability of exhaustive reports detailing the influence of coating composition and the feedstock size (nanocrystalline) on the individual corrosion and erosion behavior of a variety of coatings [8, 19, 20]. In addition, although a few review articles are also available on the erosion–corrosion performance of thermally sprayed cermet coatings, the specific erosion–corrosion response of ceramic, cermet and alloy coatings on relativistic platform, erosion–corrosion performance assessment techniques available and associated damage mechanisms as a function of operating temperature were not comprehended yet. Such a report, if made

available, is expected to serve as a ready reckoner to the researchers and practicing engineers engaged in handling the erosion–corrosion phenomenon.

In the above backdrop, various thermal spray techniques, associated process fundamentals and their capabilities were briefly presented in this article. The erosion–corrosion phenomenon and synergism to understand the erosion–corrosion interaction at microscopic level have been discussed in detail. Further, the simulation and modeling approaches available to understand the erosion–corrosion were crisply presented. The typical erosion–corrosion testing apparatus developed by different research groups and associated ASTM standards to measure the erosion in the presence of corrosion, corrosion alone and synergisms at ambient as well as high temperatures have been relevantly summarized.

Various coatings, namely WC, Cr₃C₂, NiCr, nanostructured, stellite and oxide-based coatings deposited by plasma, HVOF and DSC for erosion–corrosion/oxidation resistance applications, have been comprehensively reviewed; associated wear mechanisms and wear maps are presented. As an outcome of analysis of the literature, the available methodologies to enhance the overall erosion–corrosion/oxidation resistance of coatings at a range of temperatures through different post-coating treatments, layered coatings and resultant optimization of environment in the power generation boiler were also presented. Such an understanding thereby generated was utilized to (a) summarize the erosion–corrosion behavior as a function of operational temperature, (b) identify relevant strategies for functional performance enhancement and (c) portray the future scope of R&D in this field.

2 Thermal Spray

In thermal spray process, the material to be coated (feedstock) in the form of wire, rod or powder is passed through the high-temperature zone where the feedstock gets heated, and then, the molten/semi-molten droplets formed are propelled onto the target substrate with the help of high-speed gas jet to form a coating [21–24]. Based on this phenomenon, several thermal spray variants have been evolved based on the source of feedstock heating and particle acceleration levels as shown in Fig. 1. By and large, the source of thermal energy can be the combustion of air–fuel mixture or electrical discharge. The thermal energy produced through combustion of fuels has become the basis for development of flame spray, high velocity oxy-fuel (HVOF), high velocity air fuel (HVOF) and detonation spray coating (DSC) techniques while the electrical discharge results in evolving wire-arc spray (WAS),

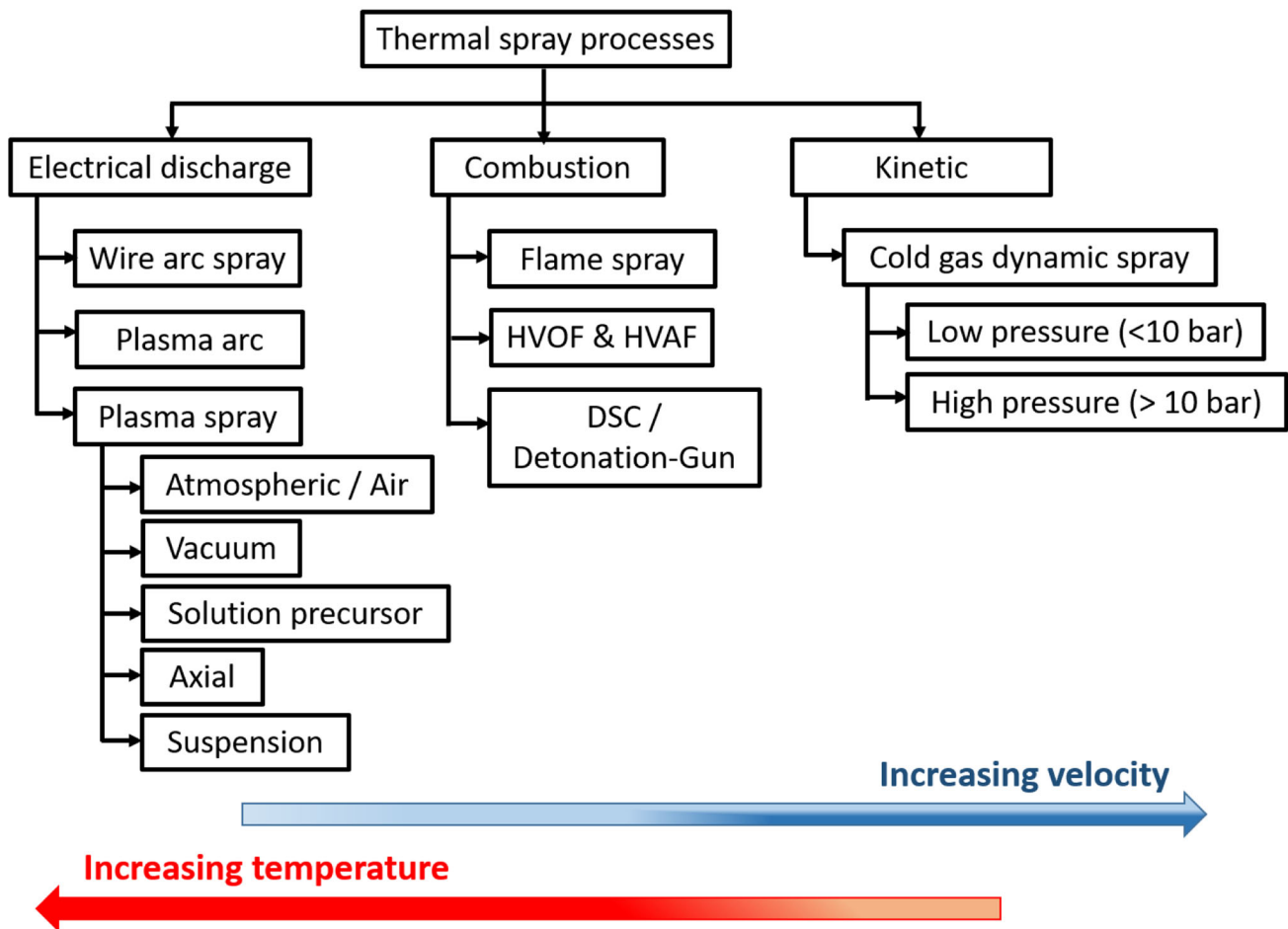


Fig. 1 Classification of thermal spray variants based on thermal energy source and corresponding kinetic energy levels

plasma transferred arc (PTA) and air plasma spray (APS) techniques.

Kinetic spray (KS) or cold gas dynamic spray (CGDS) or simply the cold spray (CS) is a recent spin-off thermal spray variant wherein the process involves significantly lower thermal energy (less than 500 °C) and higher kinetic energy (up to 1200 m/s) of particles being sprayed [21–24]. In cold spray, the gas (air, argon, helium or nitrogen) passes through a converging–diverging nozzle, resulting in the generation of high velocity carrier gas. The particles entrained in the gas are simultaneously accelerated by the high velocity gas where they impact on the substrate and eventually form adherent deposits. More details of cold spray process can be found elsewhere [25, 26]. The process fundamental of APS, HVOF and DSC, which are more relevant in the present context, has been briefly discussed in the following section along with its characteristic coating structure.

2.1 Atmospheric Plasma Spray (APS)

In plasma generated system, the argon gas is passed through a water-cooled tungsten cathode and concentric copper anode. The electrical discharge generated by passing the direct current (DC) drives the ionization of argon gas, producing a plasma [21]. The resultant plasma acts as a reservoir of thermal energy source for heating the powder feedstock; heated particles are then directed onto the substrate by purged inert carrier gas (N₂, Ar). The typical temperatures developed in the core of the plasma can be as high as 10,000 °C. Depending upon the residence time of the particle in the plasma plume, most particles will be in molten state and can attain velocities up to 200–300 m/s. This technique is predominantly used for depositing high melting materials such as ceramics and non-reactive materials. Several variants of plasma spray systems, namely vacuum, low pressure and high pressure as shown in Fig. 1, are commercially available. The selection of each system depends upon the material to be coated and application specific properties of the resultant coatings. In addition, the solution precursor plasma spray (SPPS),

suspension plasma spray (SPS) and axial plasma spray (Axial PS) are the emerging techniques in the plasma spray family [27–29].

2.2 High Velocity Oxy/Air–Fuel Spray (HVOF/HVAF)

High velocity oxy-fuel spray technique has become most popular in the last three decades to deposit a variety of wear and corrosion-resistant coatings. In HVOF process, the fuel reacts with oxygen in the hypersonic combustion gun in which a high energy thermal flux is continuously produced through high pressure combustion reaction; the feedstock loaded in a pressurized powder feeder is then traversed through the combustion chamber where the powder particles are heated up and then accelerated by the converging–diverging nozzle onto the substrate resulting in the formation of a dense coating layer [21, 30]. Like in the case of APS system, various types of HVOF spray systems such as gaseous fuel based (HV-2000, JetKote and Diamond Jet) and liquid fuel based (JP-5000, JP-8000, WokaJet-410, WokaStar-610) are commercially available in the market and more details are available elsewhere [21, 31].

The particles typically attain a temperature up to 2000–2500 °C depending on the material composition and can be accelerated up to 750 m/s. As particle attains higher velocity and significantly lower temperature as compared to the plasma spray technique, HVOF is widely used for depositing cermet (WC and Cr₃C₂-based) coatings for wear-resistant applications. It is also noteworthy to say that the carbide phase retention (minimized decomposition) is substantially better in HVOF than the plasma sprayed equivalent coatings [32]. Along with the notable extent of carbide phase, decomposition and porous microstructures in plasma sprayed coatings are known to reduce the wear resistance. Similar to HVOF, high velocity air fuel (HVAF) system has recently gained attention and is used to deposit cermet and alloy coatings with further reduced thermal energy than the HVOF. Further, owing to the significantly higher deposition rates and deposition efficiencies, the cost of spraying is substantially reduced in HVAF over the HVOF process that becomes an added advantage [33–35].

2.3 Detonation Spray (DSC)

In contrast to the other thermal spray variants, detonation spray coating is a pulsed/cyclic process in which pre-measured quantities of oxy-fuel gas mixture fill the combustion chamber located near the closed end of a 1500-mm-long barrel. The oxy-fuel mixture in the combustion chamber is ignited with a spark plug. The shock waves generated will propagate through the barrel,

eventually forming a detonation wave front that travels typically at a velocity of around 1200 m/s with its temperature around 3800 °C. The powder charged in the detonation wave gets accelerated toward the open end of barrel and eventually impinges on the substrate to form a coating [36]. Immediately, entire barrel is purged with the nitrogen gas to drive away all the residual combustion products in the barrel. Then, the system is ready for next cycle to continue the coating deposition to form thicker coatings.

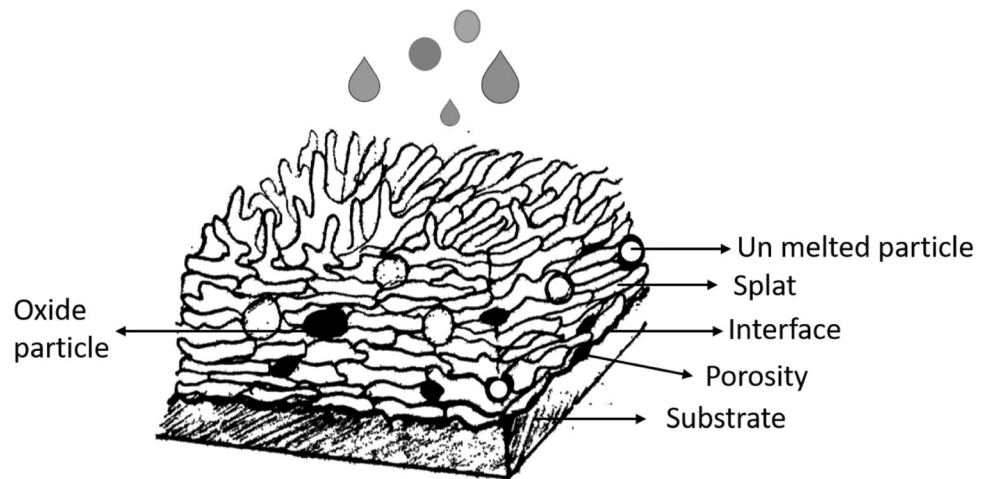
Some of the advanced detonation spray coating system can be operated up to 20 shots/s (Hz) through computer control module while the conventional systems operate typically at 3 Hz frequency. Due to its inherent higher kinetic energy offered to the feedstock particles, dense coatings with superior wear and corrosion properties can be achieved using detonation spray system. The particle velocity and temperature ranges attained in DSC are identical to that of HVOF spray system, and therefore, both DSC and HVOF are popularly used for depositing WC, Cr₃C₂ cermet coatings. In addition, the specific ability of DSC process to accommodate oxidizing, reducing and neutral environments by way of adjusting its oxy/fuel ratios enables depositing alloy coatings, metallic coatings, many ceramic oxides like Al₂O₃, Al₂O₃-TiO₂, Cr₂O₃-Al₂O₃, Y₂O₃ coatings as well [37–39].

2.4 Coating Characteristics

The typical thermal spray coating exhibits a lamellar structure with one particle flattened over the other wherein each flattened powder particle is usually referred to as “Splat.” Accordingly, a typical thermal spray coating cross section as shown in Fig. 2 consists of multiple stacked molten splats with inter-splat boundaries. The microstructure of thermal spray coating is characterized by the porosity at the splat boundaries, un-melted particles, oxides formed during exposure to flame [23]. Therefore, the properties of thermal spray coatings are certainly inferior as compared to the corresponding bulk material of identical composition. However, a dense coating with less porosity and good inter-splat bonding significantly reduces the extent of such a degradation [40].

In order to achieve such a dense coating, the process parameters have to be optimized for each coating composition to be deposited. Heat flux/oxy-fuel volume/ratio, standoff distance (distance between component to be coated and gun exit), powder feed rate are the major parameters to influence the coating properties [41]. In addition, powder manufacturing route and powder size range also influence the quality of thermal spray coatings [42, 43]. Further, the properties such as hardness, elastic modulus, coefficient of thermal expansion, melting point of coating material in relation to the

Fig. 2 Schematic of typical cross section of thermal spray coating with various characteristic features



corresponding substrate material become an important consideration. Therefore, proper optimization of process parameters to obtain dense coating is very essential for depositing coatings by thermal spray techniques. Further, understanding the coating microstructure is also crucial in adjudging its properties and performance as suggested by Wright [9]. Despite having various characteristic inhomogeneous features in a typical coating microstructure, deposition parameters should be carefully chosen beforehand such that the properties and performance of thermal spray coatings become properly correlated with their microstructure.

Since the interface bonding being provided by mechanical interlocking, cleaning of the component surface from oil, dirt and roughening of surface by grit blasting before coating deposition is the key to produce well-adherent coatings [44]. The grit type and blast pressure will also influence the coating's surface roughness and the overall quality of interface bonding (coating/component interface) [23]. An optimum grit blasting conditions that result in 4–8 μm surface roughness (R_a) is generally regarded as an essential condition to achieve good interface bonding in thermal spray coatings. Hence, a suitable combination of material, process, and optimized spray conditions and external parameters are essential to achieve high performance coatings. Therefore, based on the above results, it is understandable that the coatings with a homogeneous microstructure exhibiting a better combination of hardness, toughness, reduced porosity and improved inter-splat bonding tend to exhibit superior erosion resistance.

With regard to the coating composition, improved corrosion resistance can be tailored by the addition of selective elements that drives the formation of a well-adherent, protective surface layer. Therefore, an integrated approach encompassing the aforementioned microstructural aspects on the one hand and the compositional effects on the other is a quite useful direction. Under the umbrella of such an

integrated approach, judicious selection of deposition technique, processing parameters, feedstock powder and therefore the coating composition along with the resulting microstructure are the key variables to be explored for the successful design and development of erosion–corrosion-resistant surfaces [8, 19, 20, 45].

3 Erosion–Corrosion

Erosion–corrosion phenomenon has become an important performance benchmark due to its severity in causing damages to the typical high-temperature industrial components such as turbine blades, coal-based fluidized bed combustors, heat exchanger tubes, evaporator tubes, etc. Under the corrosion environment alone, a material can undergo either an active corrosion or exhibit passivity, while under normal erosion conditions, the surface damage is driven by the continuous impingement of solid erodent particles. In contrast, some of the components suffer from severe material loss due to simultaneous action of both corrosion and erosion referred as “erosion–corrosion (E–C).” The higher magnitude of E–C rate/loss as compared to the sum of material loss due to erosion alone and corrosion alone in many situations can be attributed to synergistic effect of erosion on corrosion and vice versa [7, 8]. Such an unusual behavior can be rationalized based on the fact that, under the action of erosion–corrosion, the protective oxide layer even if formed due to corrosion can quickly get damaged because of continuous bombardment of erosion particles. In addition, the active corrosion phenomenon as triggered by the subsequent loss of protective layer in combination with the availability of rough and damaged/eroded area can significantly increase the E–C rate [8]. Therefore, a systematic approach that is needed to understand the synergistic effect of erosion and corrosion is provided in the following section.

3.1 Erosion–Corrosion Material Loss Analysis

Material loss due to erosion–corrosion is a complex phenomenon, which involves synergism of erosion–corrosion along with pure erosion and corrosion affect. The quantification of erosion–corrosion data and their synergy has been carried out based on ASTM G119 [46–48] by the following equations along with their constituent parts:

$$W_{EC} = W_{E0} + W_{C0} + W_S \quad (3.1)$$

where W indicates the wear loss and subscript EC is the total material loss due to erosion–corrosion, E0 is the pure erosion, C0 is the pure corrosion, S is the synergic wear due to effect of corrosion on erosion and erosion on corrosion as further defined below:

$$W_S = \Delta W_{CE} + \Delta W_{EC} \quad (3.2)$$

where ΔW_{CE} is the effect of corrosion on erosion rate (synergistic effect) implying the increase in mechanical wear due to corrosion and ΔW_{EC} is the effect of erosion on corrosion rate (additive effect) referring to corrosion of material due to concurrent erosion. Although the above approach is used for many applications, it becomes more challenging under high-temperature conditions due to the oxide formation on non-exposed surfaces; possibility of embedded erodent leading to weight gain hence requires a new methodology to assess the wear loss, corrosion and synergism. Therefore, material loss calculations based on the metallographic analysis of cross sections eliminate the overestimation of coating thickness due to the presence of residual oxides that appear to be more sensible. At the same time, such a metallographic analysis can be very tedious, as the overall accuracy of wear loss measurements is proportional to the number of sectioned areas examined to obtain a statistically acceptable erosion loss data. In order to measure the individual contributions to the overall material loss, various erosion–corrosion test rigs working under jet impingement, fluidized bed, whirling arm designs coupled with in situ electrochemical measurements were developed [4, 6, 49] and the following section provides such details.

3.2 Test Setup

Due to complex nature of erosion–corrosion material loss as discussed before, different test equipments are designed to measure the material loss due to combined and individual contributing factors during erosion–corrosion [6, 47, 50]. Typical erosion–corrosion (E–C) testing involves directing the solid particle erodent at a particular velocity and feed rate to impact onto the sample that is held in the corrosion environment and positioned at specified standoff distance and at an angle. It may be noted that, in

the case of erosion–corrosion, the solid abrasive particles are mixed with the aqueous corrosion medium and then accelerated to impinge the sample surface, whereas in the case of erosion–oxidation, the sample will be exposed to high temperature in a chamber that circulates the flue gases while being impacted by the solid particles. Several simulated erosion–corrosion test rigs are designed to facilitate the conditions that replicate the real-time application environment such as the conditions that are prone in a typical power plant [51–53]. The details about various test rigs reported in the literature have been discussed in this section.

The most popular test rigs for erosion–corrosion measurement are categorized broadly into two types [6]. In the jet impingement type, E–C testing apparatus consists of a nozzle through which the erodent particles with a predefined velocity are directed onto the sample surface. For carrying the solid particles, a jet/stream of gas or liquid is used to impart the predefined velocities. In addition, the erodent should be discharged at specified rate (loading rate) through the erosion-resistant nozzle. The sample is fixed in the holder and then positioned at a particular distance from the nozzle exit and at a given angle of impingement. The other popular design involves a rotary nozzle driving an impinging fluid jet on the sample surface due to centrifugal force [4]. The major test parameters that influence the overall erosion–corrosion rate include velocity, impingement angle, flow regime, standoff distance, corrosion medium and its concentration (pH), temperature, nozzle diameter, test duration, erodent discharge/loading rate, erodent–material and its shape, size distribution and the relative hardness [6, 14, 54–56].

It is to be noted that the erosion–corrosion test rig should consist of three-electrode potentiodynamic polarization setup within the erosion test chamber itself to measure the material loss due to corrosion alone. A 3-electrode system which consists of working electrode (material under study), standard electrode (SCE) and counterelectrode (platinum) is used for measuring the corrosion rate. In order to measure the pure mechanical wear loss of sample in the presence of corrosion medium, it is recommended to polarize the specimen at 1.0 V cathodic potential with respect to E_{COR} to avoid any active corrosion of the sample [57]. However, such a value of cathodic potential depends primarily on the nature of the material to be tested. For instance, in the case of WC–Co coating tested in 3.5 wt% NaCl solution, a cathodic potential of 0.8 V is reported as a suitable condition to arrest the corrosion instead of 1.0 V as recommended by ASTM G119 standard [47, 57]. Hence, a simple and best-designed test rig is required to measure the erosion and corrosion loss of material as well as loss due erosion–corrosion synergism. Further, due to complex nature of erosion–corrosion phenomenon, modeling and

simulation studies (empirical, mathematical and numerical) are also actively performed to understand the material loss mechanisms at both microscopic and macroscopic levels, and then, corresponding results are compared through experimental design and analysis [7].

Similar to erosion–corrosion measurement at room temperature as presented so far, different test rigs are employed to study the erosion–oxidation behavior of bulk as well as coatings at high temperatures. Three types of test rigs have been reported to study the erosion–oxidation behavior, viz. fluidized bed (FB) rig, jet impingement rig and rotating rig. The schematic of these test rigs is provided in Fig. 3 [4]. FB rigs are designed to simulate the fluidized bed combustion chamber, whereas jet impingement rigs are designed to simulate the coal-fired boiler or gas turbine engines. As a common feature to all the test rigs, heating of gas by either fuel or electrical means results in injection on particles in the hot gas steam which accelerates and impacts the substrate surface. It is noteworthy that each test has its own merits and demerits. For instance, it is easy to pass gases in the FB test rig as compared to the other two test rigs. However, the velocity attained by the particles is limited in FB test rig, i.e., up to 15 m/s. Further, each test rig is having different modules, namely a rotating or reciprocating sample module of FB test rigs, whirling arm and centrifugal module in case of rotating rigs. The advantage with centrifugal test rig has been its ability to host a number of samples at different impact angles in a single test itself and therefore is widely used to study the erosion–oxidation of bulk materials and coatings. More details about the basic operational features and associated principles are found elsewhere [4].

4 Erosion–Corrosion Resistant Coatings

Thermally sprayed WC and Cr_3C_2 -based (cermet) coatings have been widely investigated for their wear and corrosion resistance. The specific erosion–corrosion behavior of these cermet coatings has been detailed in this section. Accordingly, the influence of coating type and matrix composition on the erosion–corrosion behavior has been discussed. Further, the choice of materials and coating combinations have been selected in a way that their erosion–corrosion/oxidation behavior has a direct relevance for boiler materials in power plants. More importantly, the associated material removal mechanisms during the ambient, high-temperature erosion–corrosion/oxidation and corresponding wear maps have been presented and analyzed to portray the future direction of R&D in the following subsections.

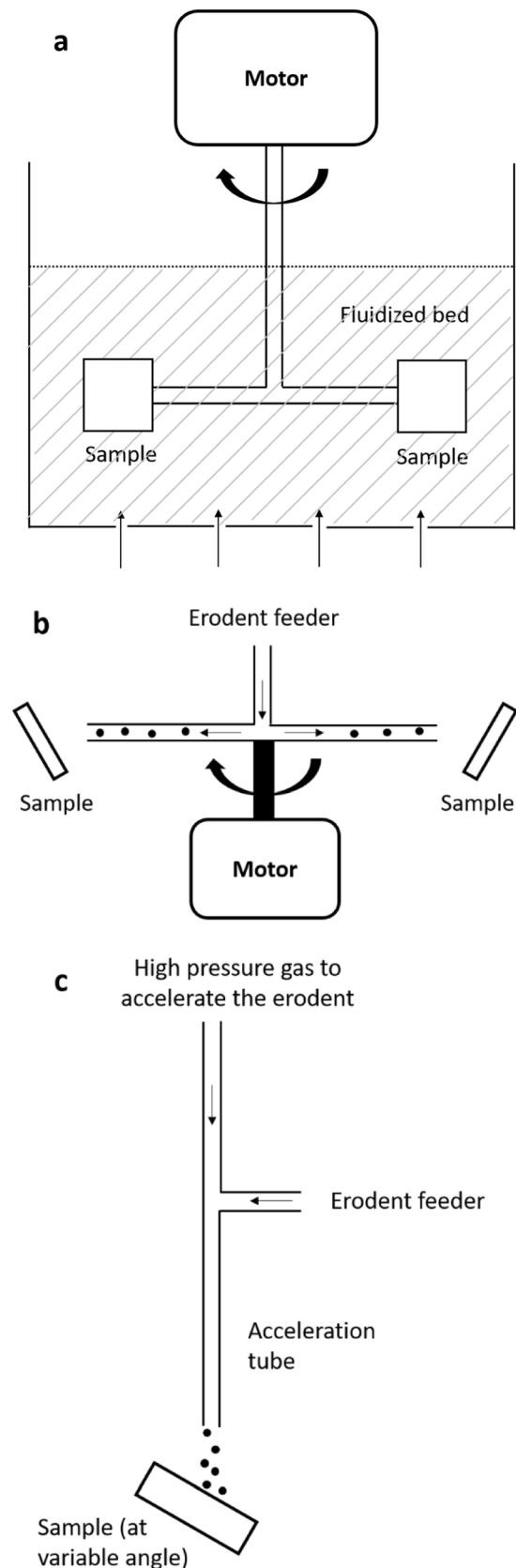


Fig. 3 Schematics of high-temperature erosion–corrosion/oxidation test rigs, namely **a** fluidized bed—FB type, **b** rotating centrifugal type and **c** jet impingement rig [4]

4.1 Ambient Temperature Erosion–Corrosion

WC-based cermet coatings deposited through HVOF and DSC are employed for the components such as ball valves, gas turbine blades, pump impellers and others those usually encounter erosion–corrosion damage. For example, Fig. 4a, b illustrates the uncoated and WC–Co-coated superduplex stainless steel impeller after its service in water. The coated impeller exhibits negligible damage at the eye wear ring after 9½ months of service illustrating the efficacy of WC–Co coatings to protect the components from erosion–corrosion damage [58].

The erosion–corrosion behavior of WC coatings as a function of hard phase size, matrix composition, feedstock size distribution, erodent proportion, rotation/peripheral velocity and corrosive medium has been studied in detail [57–60]. The erosion–corrosion tested WC–17Co coatings typically demonstrate a 22% reduction in the material loss as compared to the uncoated AISI 1018 steel under the simulated test conditions of 3.5 wt% NaCl + 1000 ppm NaHCO₃ + 1 wt% silica (100 µm). However, the

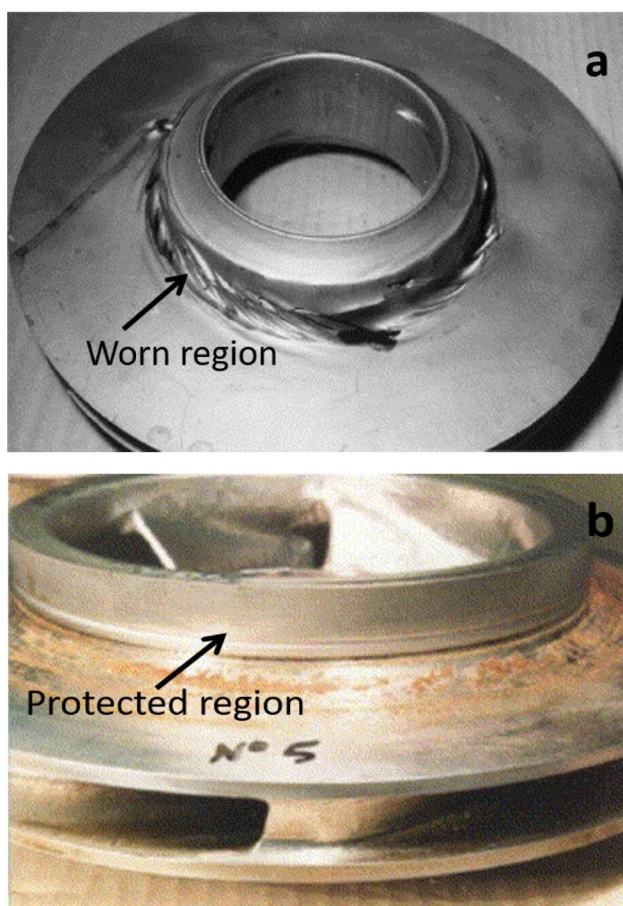


Fig. 4 Superduplex stainless steel (UNS S32760) impeller **a** uncoated and in service for 7 months and **b** WC–Co coated and in service for 9½ months [58]

corrosion resistance of WC–Co coatings is not up to the mark, as limited by the presence of corrosion-prone Co matrix. A near-nanocrystalline duplex WC–17Co feedstock is prepared through a special route comprising of mechanical milling + spray drying + chemical vapor deposition (CVD). Such a duplex feedstock when sprayed using HVOF process results in further decrement in the erosion–corrosion rate to ~ 70% and ~ 30% than the corresponding bare steel substrate and conventional (microcrystalline) WC–17%Co coating, respectively. Such an enhancement in E–C resistance of near-nanocrystalline coating is due to more compact structure with less intersplat porosity and reduced micro-cracks which is otherwise noticed on the microcrystalline coatings. In addition, higher hardness (HV1440) as compared microcrystalline WC–17Co coating (HV1048) has also contributed to the considerably reduced E–C damage [61]. Furthermore, the WC size also influences the erosion–corrosion rate of WC–Co–Cr-based coatings. The finer the WC grain in WC–Co–Cr coatings (WC around 1 µm), the better is the erosion–corrosion resistance. The presence of such finer WC grains in the coating, as compared to the coarser grain WC–Co–Cr coatings (WC around 5 µm), perform better under E–C conditions primarily due to uniform distribution of WC in metal matrix causing lesser dislodgement of WC grains during erosion [60].

Further, Co replaced with Ni in WC-based cermet coating exhibits better electrochemical corrosion resistance than WC–Co coating. However, the erosion resistance of WC–Ni coating is notably inferior to that of WC–Co coating [60]. Although the WC–Ni coating possesses relatively poor erosion resistance as compared to the WC–Co coating, the erosion–corrosion resistance of WC–Ni coating is surprisingly found to be superior to WC–Co coating due to Ni, which is relatively nobler than Co [60]. Further, the WC–Ni coatings also exhibit better E–C resistance than the Cr₃C₂–NiCr coatings that are well known for their superior corrosion resistance in 3.5 wt% NaCl solution [45, 60]. The surface morphologies of erosion–corrosion-tested Cr₃C₂–NiCr and WC–Ni coatings are illustrated in Fig. 5a, b. As can be expected based on uniform material loss in the case of WC–Ni coating (Fig. 5b), it shows superior E–C resistance than the Cr₃C₂–NiCr coating. The inherent high hardness of WC–Ni as compared to Cr₃C₂–NiCr coating is responsible for its superior E–C performance. Therefore, it is noteworthy that the material that performs better under static corrosion conditions need not perform similarly under erosion–corrosion conditions.

Moreover, the matrix composition in WC-based coatings should be carefully selected such that it should be compatible with the surrounding material systems. For instance, when the coated component is surrounded with more passive materials like stainless steel, the coating

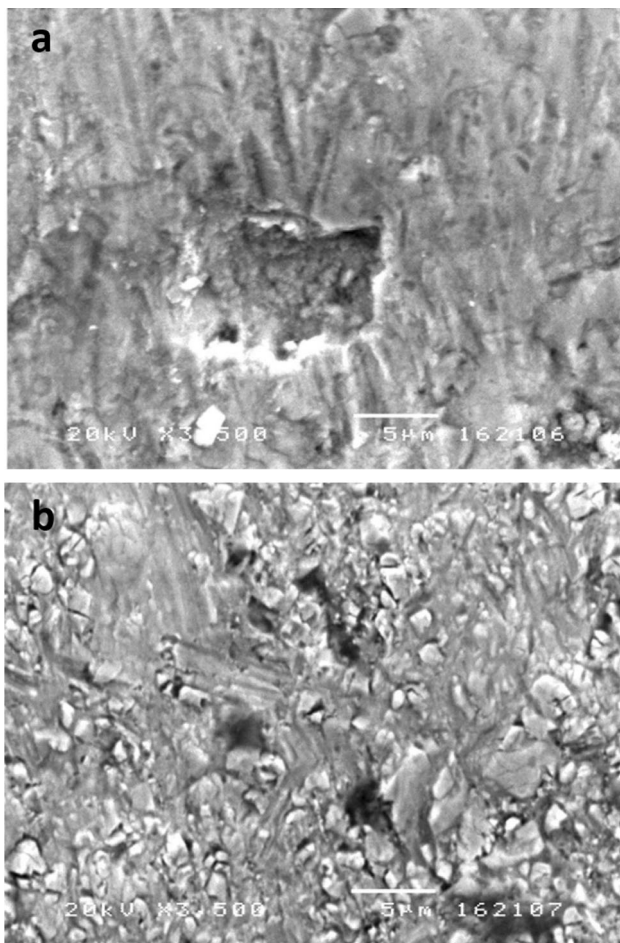


Fig. 5 SEM images illustrating the erosion–corrosion damage morphology of **a** Cr₃C₂-NiCr and **b** WC-Ni coating surfaces tested in 3.5 wt% NaCl solution and silica as an erodent [60]

becomes relatively anodic and forms a galvanic couple between coating and the surrounding material and therefore increases the corrosion damage. Such a scenario can be found in the case of pumps, pipes and valves coated with WC-based cermet coatings [8, 60, 62]. Therefore, in order to address this issue, Cr is to be added to either Co or Ni binder such that the resultant coatings become cathodic and continue to enhance the erosion–corrosion resistance and protect the stainless steel substrate.

In this direction, the WC coatings with either CoCr or NiCr matrix perform better under erosion–corrosion conditions in aqueous solution than WC-Co coatings [59, 61, 63, 64]. To further probe the influence of Cr content in the feedstock and the corresponding powder particle size distribution on the E–C resistance, the HVOF sprayed WC-Co-Cr coatings are systematically assessed in sea water medium [59]. It confirms that the Cr-containing WC-Co feedstock (WC-10Co-5Cr and WC-6.5Co-8.5Cr) with narrow particle size distribution (36-45 μm) exhibits lower erosion–corrosion damage owing to the uniform

heating of the in-flight particles and better retention of WC phase in the coating, as clearly illustrated in Fig. 6a, b [59]. At the same time, although the Cr content is beneficial for better E–C resistance, a higher Cr content in the binder matrix will be beneficial under less aggressive erosive conditions (at 14.3 m/s rotational velocity of fluid containing 3.4 wt% NaCl and 0.25 wt% silica sand) where the corrosion rate controls the overall mass loss. In contrast, under more aggressive erosive conditions (22.9 m/s rotational velocity), the erosion wear resistance of the coating plays a significant role in adjudging the erosion–corrosion resistance of WC-Co-Cr coatings [59]. This clearly highlights the fact that the knowledge of component working conditions is necessary to design and select an appropriate composition.

The influence of erodent proportion and temperature of the NaCl medium on the erosion–corrosion behavior of WC-12Co-6Cr coatings deposited through HVOF and Super D-Gun was investigated [57]. As one can expect, the rate of erosion–corrosion increases with the increasing erodent concentration, but the influence of temperature rise

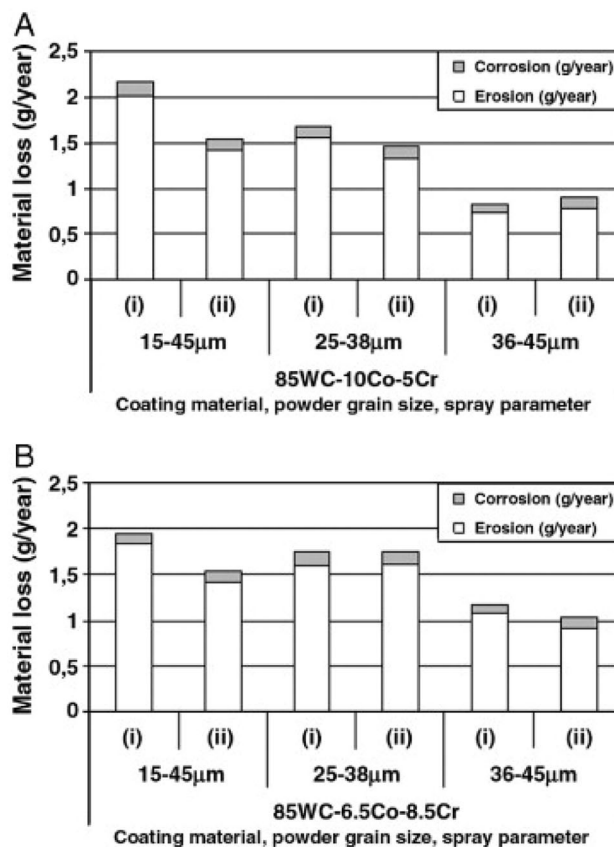


Fig. 6 Erosion–corrosion material loss of HVOF sprayed WC-Co-Cr coatings as a function of feedstock powder size distribution and matrix composition **a** 85WC-10Co-5Cr and **b** 85WC-6.5Co-8.5Cr wherein (i) and (ii) indicate two different spray distances, namely 230 mm and 180 mm, respectively [59]

from 20 to 50 °C of NaCl solution on the erosion–corrosion rate of WC–12Co–6Cr coating is relatively significant. An increasing erosion–corrosion rate with increasing jet velocity has been verified [59]. It may also be noted that the test duration and type of corrosion medium strongly influence the E–C behavior of cermet coatings. For instance, irrespective of coating type (WC–Co or CeO₂-modified WC–Co), the E–C rate is significantly higher in 3.5 wt% NaCl than 1 mol/l H₂SO₄ corrosion medium up to 4 h of test duration. In contrast, beyond 4 h test duration, both the coatings demonstrate high E–C rate in 1 mol/l H₂SO₄ solution. Such an unusual behavior is explained based on the absorption and osmosis nature of aggressive SO₄[−] ions into the micro-cracks of the coating resulting in inferior E–C resistance during prolonged test duration [65].

4.1.1 Erosion–Corrosion Maps

There is an increasing interest to understand the material loss mechanisms in multi-dimensional space on the erosion–corrosion behavior of thermal spray coatings whether mechanical or electrochemical property to be improved is based on the service environment. An attempt has been made by V.A.D. Souza et al. to study the individual damage mechanism (either erosion (*E*) or corrosion (*C*) and synergy (*S*) dominance) by plotting the material loss caused by pure erosion (*E*) against the material loss due to combined corrosion and synergy (*C* + *S*). Under ambient temperature (20 °C), the rate of material loss increases significantly with the erodent concentration and eventually degradation mechanism changes from pure erosion dominance to erosion–corrosion interface regime as shown in Fig. 7 [1, 58]. Interestingly, the material loss suffered due to corrosion with increasing temperature from 20 to 50 °C of NaCl solution shifts the wear loss from pure erosion dominated to erosion–corrosion dominated regime for all erodent concentrations studied. Similarly, Wood et al. reported the E–C maps for HVOF sprayed nickel aluminum bronze (NAB) coatings on carbon steel where the NAB coatings clearly exhibit better erosion–corrosion resistance than the carbon steel substrate [66].

Stack et al. studied the erosion–corrosion behavior of HVOF sprayed WC–Co–Cr coatings as a function of impact velocity, slurry concentration and applied potentials in aqueous conditions [2, 67, 68]. The erosion wear loss mechanisms, erosion–corrosion synergy, erosion–corrosion additive synergy maps were developed for WC–Co–Cr coatings. The erosion–corrosion performance maps of mild steel and WC–Co–Cr coatings at 2 and 4 m/s impact velocities are shown in Fig. 8. At 2 m/s impact velocity, under cathodic conditions, the coating and the mild steel can be used for all erodent concentrations (200 mg/l to 1000 mg/l). However, at higher potentials, WC–Co–Cr

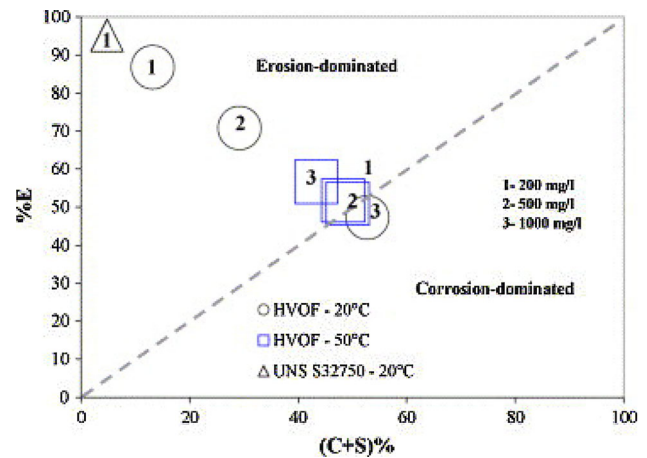


Fig. 7 Influence of erodent concentration and temperature on the erosion–corrosion of HVOF sprayed WC–Co–Cr coatings and UNS S32750 steel [58]

coating performs significantly better than the mild steel at both velocities and the range of erodent loading conditions [2].

It may be noted that the aforementioned material degradation maps are plotted based on the synergy concept as discussed previously (Sect. 3.1). However, a wide range of interaction is noticed within the erosion–corrosion test parameters. Nevertheless, the major material loss is due to the mechanical action than the corrosion observed in WC–Co–Cr coating in aqueous solutions. The detailed synergistic and antagonistic (negative synergistic effect) mechanisms in case of WC-based coatings have also been reported recently [8, 66]. Various studies reported so far clearly concludes that the erosion–corrosion phenomenon is more complex as it is influenced by a number of test parameters and of course the coating composition. Hence, there is a need to develop such maps for variety of candidate coatings such that an effective selection of suitable coating material for a particular component material and corresponding environment combination is possible.

4.1.2 Coating Removal Mechanisms

The coating removal mechanisms are mostly sensitive to the coating microstructure. The microstructure of thermally sprayed WC and Cr₃C₂ coatings is more complex than corresponding bulk material microstructure. For instance, the microstructure of WC–Co coating deposited by DSC as shown in Fig. 9 consists of WC carbides embedded in cobalt matrix (bulk materials) along with mixed Co matrix phases such as Co_xW_xC, W₂C, partially amorphous matrix phase, inter-splat boundaries and porosity [69]. The erosion–corrosion mechanism in WC–Co coating involving the loss of integrity between matrix and hard phase particles due to preferential dissolution/corrosion of matrix

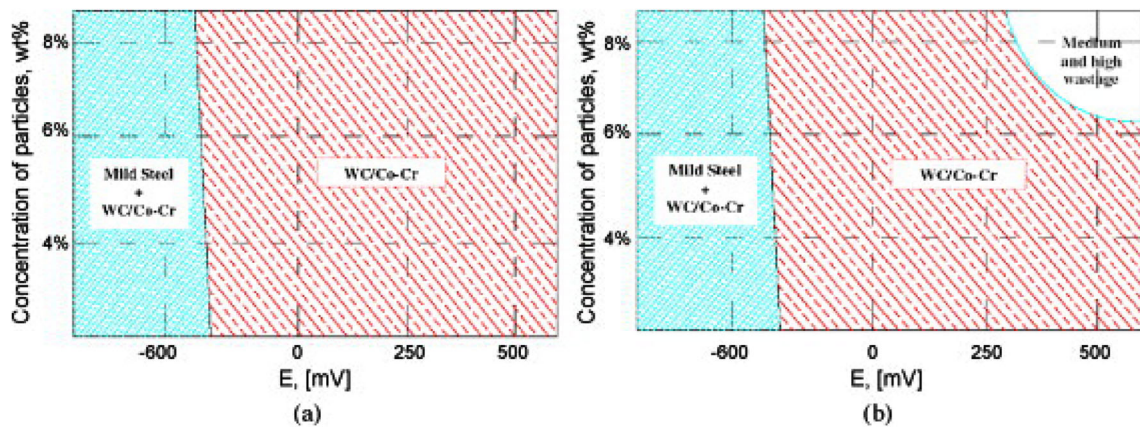


Fig. 8 Erosion–corrosion maps for HVOF sprayed WC–Co–Cr coatings at **a** 2 m/s and **b** 4 m/s impact velocities [68]

phase followed by the removal of hard phase eventually causing the thinning of coating is schematically shown in Fig. 10 [58, 61, 70]. Therefore, relatively higher erosion–corrosion loss of WC–Co coating is understandable [57–60]. Although the material removal mechanism in WC–Co–Cr coatings is identical to WC–Co coatings, the presence of Cr in WC–Co–Cr coatings promotes the formation of a thin Cr₂O₃ passive layer on its surface that enhances the overall erosion–corrosion resistance under less aggressive erosion conditions. However, it is to be noted that when the erosion–corrosion conditions promote the material removal rate in excess of oxide formation rate, i.e., under aggressive conditions, such a protection offered

by the presence of “Cr” in the coating becomes redundant [45, 59, 71].

4.1.3 Strategies to Enhance the Erosion–Corrosion of WC–Based Cermet Coatings

In general, E–C rate of a cermet coating is higher due to the matrix’s preferential corrosion susceptibility. Therefore, toward enhancing the E–C resistance without compromising the mechanical properties, the matrix compositions as well as carbide-based ceramic hard phases are partially or considerably modified/substituted with more corrosion-resistant phase combinations. Accordingly, the addition of about 4 wt% Cr to WC–10Co exhibit better erosion–

Fig. 9 Surface morphologies of thermally sprayed **a** WC–Co, **b** WC–Co–Cr, **c** WC–Cr–Ni and **d** Cr₃C₂–NiCr coatings [69]

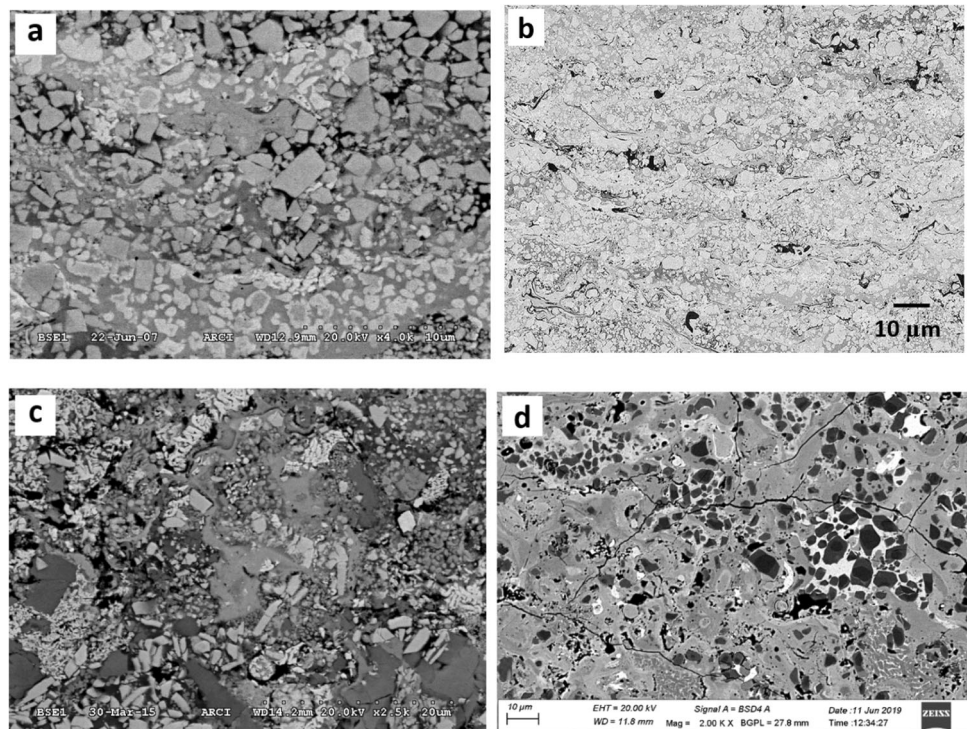
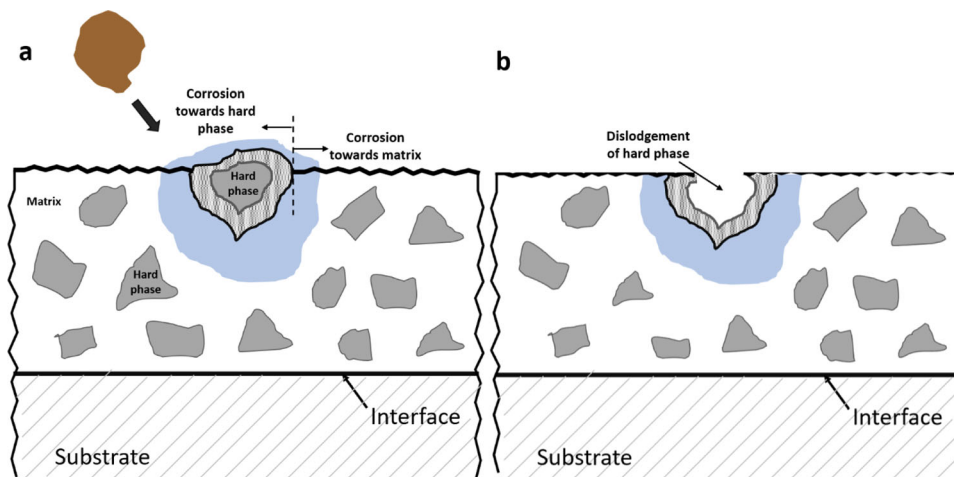


Fig. 10 Schematic of material loss in WC–Co–Cr coating **a** during impact and **b** after impact showing dislodgement of WC particle



corrosion resistance. Further, HVOF sprayed WC–Co and CeO₂-modified WC–Co coatings erosion–corrosion performance has been comparatively evaluated in two different corrosion media, namely 3.5 wt% NaCl and 1 mol/l H₂SO₄ mixed with an erodent silica sand of 500 μm size. Owing to the reduced porosity, the CeO₂-modified WC–Co coating exhibits lower corrosion rate and higher E–C resistance than the conventional WC–Co coatings in both the corrosion media. In contrast, the corrosion rate of WC–Co coating as measured through polarization studies is lower in H₂SO₄ medium as compared to CeO₂-modified WC–Co coating while it is identical in NaCl solution. This behavior suggests that the simple (both immersion and polarization) corrosion tests are not adequate to assess the overall erosion–corrosion rate of a material/coating [65]. Similarly, addition of Inconel 625 to HVOF sprayed nanostructured WC–12Co coating results in better E–C resistance due to the formation of passive film derived out of the constituents from Inconel 625 [17]. By resorting to post-treatment methods such as boron nitride sealing, polymer impregnation, furnace fusing, laser melting and cathodic protection, enhancement in the overall E–C resistance of thermal sprayed coatings is noticed [72–76].

4.1.4 Comparing the Erosion–Corrosion Behavior of Cermet and Other Coatings

The comparative erosion–corrosion behavior of HVOF sprayed WC–Co–Cr, Cr₃C₂–NiCr and Al₂O₃ coatings was evaluated in 3.5 wt% NaCl solution as a corrosion medium and 355 μm angular silica as an erodent [77]. Despite having high corrosion resistance, the Cr₃C₂–NiCr coating demonstrates poor E–C resistance due to its inherently lower hardness and wear resistance as compared to WC–Co–Cr and Al₂O₃ coatings (Fig. 11). The carbide pull-outs in the Cr₃C₂–NiCr coating eventually mixes with the erodent and lead to an increase in the erosive nature resulting

in inferior E–C resistance of Cr₃C₂–NiCr coating than the bare EN steel substrate. Least erosion scar depth has been identified for WC–Co–Cr coatings than the other two coatings. Among the carbide-based cermet (Cr₃C₂–NiCr and WC–Cr₃C₂–Ni) and oxide-based ceramic (Cr₂O₃–Al₂O₃–TiO₂ and Cr₂O₃) coatings evaluated in 0.1 M NaOH + 100 g/l silica medium at a velocity of 2.35 m/s for 48 h, the Cr₃C₂–NiCr cermet coating demonstrates superior E–C resistance, though its generic corrosion resistance is lower as compared to the oxide-based ceramic coatings. Furthermore, among WC–Cr₃C₂–Ni and Cr₃C₂–NiCr cermet coatings, WC–Cr₃C₂–Ni exhibits low corrosion and E–C resistance in alkaline (NaOH) medium due to the deficiency of free Cr as well as the low hardness compared to Cr₃C₂–NiCr coating. To summarize, the E–C performance order of various coatings in terms of their resistance to erosion–corrosion is WC–Co–Cr > Cr₃C₂–NiCr > Cr₂O₃–Al₂O₃–TiO₂ > Cr₂O₃ > WC–Cr₃C₂–Ni

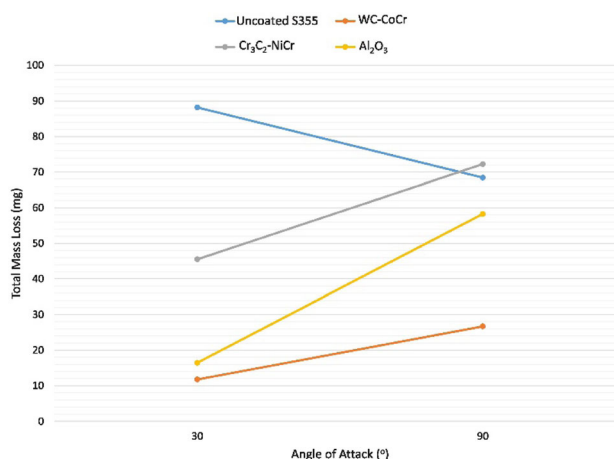


Fig. 11 Erosion–corrosion loss of different coatings in comparison with the substrate as a function of erodent angle [77]

(with silica as erodent in NaCl and NaOH corrosion media) [63].

It is apparent that among WC and Cr₃C₂-based cermet coatings, the coating composition must be chosen in such a way that it should possess possible high hardness (wear resistance) in combination with the free Cr availability in the matrix (to promote the formation of protective oxide layer) to improve its erosion–corrosion resistance. It can be concluded that, under ambient temperatures, the WC-based cermet coating (especially with CoCr as matrix) exhibits high E–C resistance than the Cr₃C₂-based coatings while the order of merit reverses at higher temperatures up to 900 °C [8]. In view of the above, it may be noted that the erosion–corrosion resistance of thermally sprayed WC and Cr₃C₂-based cermet coatings can be enhanced by high fraction of carbide phase, good bonding between matrix–carbide interface and proper inter-splat bonding as well [58].

Further, Fe-based amorphous coating sprayed by HVOF exhibits better E–C properties than low-carbon nonmagnetic steel in 3.5 wt% NaCl solution with 1 wt% SiO₂ at 15 m/s velocity. Such an enhanced E–C resistance together with general wear and corrosion protection has been accorded by the presence of amorphous Fe phase in the coating. It is interesting to note that the E–C rate of Fe-based amorphous coating is almost comparable to HVOF sprayed WC–Co–Cr coatings and can use as an alternative to WC–Co–Cr coatings [78].

4.2 High-Temperature Erosion–Corrosion/Oxidation

The erosion in the presence of corrosive solution at lower temperatures is generally termed as erosion–corrosion while the similar phenomenon at higher temperatures is more commonly referred as erosion–oxidation. However, a clear temperature range delineating the erosion–corrosion and erosion–oxidation window is not available in the literature probably because different material systems respond to oxidation at different temperatures. At the same time, while the erosion–oxidation is also synonymously referred to as erosion–corrosion, the former terminology (erosion–oxidation) is used in the present article for clear distinction. In view of that, many components in power plants, gas turbine and petrochemical industry are exposed to simultaneous wear and corrosion or oxidation at high temperature; therefore, the erosion–oxidation behavior is of significant interest to the industry concerned [52, 79–81]. Similar to erosion–corrosion (at ambient temperatures), erosion–oxidation (at high temperature) is also a complex phenomenon. Therefore, to obtain the performance data, most of the tests were carried out under simulated conditions (similar to the service environment), or some times

the tests were carried out under real service conditions (by welding the samples in the actual power plant) [54, 82].

Comprehensive understanding of E–C response of a given material also demands studying the influence of erosion parameters, namely the type of erodent medium, its velocity and angle of impingement. In the erosion–oxidation process, it is expected that the particle impacts on the pre-formed oxide layer leading to either partial or complete removal of oxide layer based on the velocity of the erodent particle [1, 9]. Accordingly, the material loss is of an order of magnitude higher when eroded at 52 m/s than 19 m/s using alumina erodent at 871 °C (simulated condition of gas entering the first cyclone separators in coal combustion systems) in erosion–oxidation environments at 30° impact angle on a variety of materials [9]. In addition, the removal rate of pre-formed oxide layer is dependent on the erodent velocity. Accordingly, once the oxide layer is completely removed, then the residual coating exhibits a linear mass loss rates.

Under such a scenario, it is imperative that the material removal rate is proportional to the thickness of oxide layer removed per impact [9]. Based on the residual thickness, subsequent growth of oxide layer and concurrent removal rate vary with the parabolic growth rate of oxide. Further, the growth rate of oxide layer depends on the frequency of impacts that decides the average time available for regrowth of oxide layer between the two successive impacts. Besides, the surface temperature controls the oxidation kinetics. However, it is to be noted that the above factors are valid based on the assumption that the oxide layer is uniform; single oxide phase is formed.

A modeling approach was also attempted to quantify the mass loss in erosion–oxidation conditions to assess the erosion footprint. The model was based on Monte Carlo simulation techniques. The methodology involved the following steps: (i) a statistical distribution to identify different erosion regimes, (ii) Monte Carlo method for selecting discrete impact conditions and (iii) summing up data for erosion–corrosion under simulated gas turbine conditions. The results were found to be realistic and therefore demonstrated the potential to describe the erosion–corrosion mechanisms [7, 9]. However, the present level of understanding of erosion–oxidation based on such modeling tools is much limited; further studies are needed to understand the mechanisms on a global scale [1, 7, 9]. For example, the data required to validate the erosion–oxidation “erosion footprint model” are not completely available. Moreover, model validation requires development of complex relationships incorporating a number of properties pertaining to a particular erodent–material combination. Often, the input variables needed for designing an effective model under the E–C mode may not be independent and therefore raises the complexity further.

In general, hardness is the most determining property in adjudging the wear resistance of a coating. However, hardness alone is not an indicative tool to decide the erosion resistance as microstructure, which depends on the coating deposition technique, and spray parameters collectively influence the erosion rate. In addition to the processing parameters, the heterogeneous nature of cermet coatings turns the modeling much more difficult. Further, the complexity will increase upon interaction of corrosion or oxidation along with erosion process. Though the development of models for erosion–corrosion/oxidation is complex in nature, once they mature, it would be a lot easier to investigate the real life service issues case by case in an effective way.

In power plants, the typical components such as superheaters, re-heaters, heater boiler tubes and heat exchanger tubes are made out of alloy steels (preferably ferritic/martensitic or austenitic alloy steels) and superalloys. Among alloy steels, T22 (0.05–0.15 C, 0.5 Si, 0.3–0.6 Mn, 0.025 P, 0.025 S, 1.9–2.6 Cr, 0.87–1.13 Mo, Balance-Fe) and T91 (0.07–0.14 C, 0.2–0.5 Si, 0.3–0.6 Mn, 0.2 P, 0.2 S, 8–9.5 Cr, 0.85–1.05 Mo, 0.4 Ni, 0.18–0.25 V, 0.015 Al, Balance-Fe) are quite popular and widely used as boiler tube materials. Furthermore, T91 steel has got more Cr content, high yield strength and creep strength as compared to T22 steel [13, 82]. The influence of oxidation on erosion behavior of various boiler steels at a higher temperature under cyclical oxidation and protected atmospheres has been investigated and it has been found that an adherent, quick healing film forms on the austenitic steel [52]. However, it has also been noticed that, in majority of the cases, the material loss in steels under erosion–corrosion environment is mostly controlled by the erosion process than the corrosion/oxidation.

Having said that, it is to be noted that the surface oxide layer formed contributes to enhance the overall erosion resistance of a material especially at oblique angles. Due to the inability to work at higher temperatures (can safely operate at temperatures < 550 °C), generally these alloy steels are subjected to thermal spray coating using suitable cermet or ceramic powders and have been explored extensively in the recent years. It may be noted that only the thermal sprayed coatings tested under high-temperature gas jet erosion and in real boiler conditions are considered within the scope of this article. K. Szymanski et al. have summarized the activities on the development of erosion and corrosion-resistant thermal sprayed coatings for power plant boiler applications in Poland. Accordingly, the protective thermal sprayed coatings deposited on various power plant components are shown in Figs. 12, 13 [11].

It is to be noted that the WC-based cermet coatings can be applied for superior erosion and moderate-to-good corrosion-resistant applications up to 550 °C, while the

Cr₃C₂-based cermet coatings possess good erosion resistance and superior corrosion resistance up to 850 °C [45, 51, 83]. Upon comparing the erosion–oxidation (E–O) behavior of HVOF sprayed Ni–20Cr alloy, WC–CrNi and Cr₃C₂–NiCr cermet coatings as a function of temperature (from 100 to 850 °C) under gas jet erosion testing at different velocities, the Cr₃C₂-based cermet coating is found to exhibit superior erosion–oxidation resistance consistently up to 850 °C. Further, the material loss suffered by the WC-based cermet coating increases drastically beyond 550 °C, resulting in poor E–O resistance than Ni20Cr alloy and Cr₃C₂–NiCr coatings [84–87]. Irrespective of coating type and testing temperature, the significant increase in material loss with increasing erodent velocity from 3.5 to 14.8 m/s is observed. Interestingly, the E–O resistance of HVOF sprayed Cr₃C₂–NiCr coating can be further enhanced by spraying the nanostructured feedstock [85].

The erosion–oxidation maps corresponding to HVOF sprayed Ni–Cr, WC–20Cr–7Ni and Cr₃C₂–NiCr coatings as a function of temperature and impact velocities evaluated based on the mean surface roughness criteria can be found elsewhere [86]. Accordingly, at lower velocities (2.5 to 4.5 m/s), material loss regime is surface dominated up to 600 °C. Between 600 °C and 700 °C, the material loss is



Fig. 12 Protective coatings deposited by thermal spray in fluidized bed power boiler **a** after 1 year of operation, **b** coating regenerating process above the lining and **c** regenerated coating after 9 years of service [11]

Fig. 13 Protective thermal spray coating deposited on the rotor fan and the elements of pulverized coal burner [11]



due to oxidation-modified erosion–oxidation or erosion effected by oxidation. Beyond 700 °C temperature, the material loss of three HVOF coatings is oxidation controlled erosion or oxide-dominated erosion. Further, at higher impact velocities (11–19 m/s), erosion–oxidation loss of the three coatings is significantly higher indicating that the oxide formed on the coatings can not impede the material loss. Such observations are expected to serve as guidelines for selection of proper coating material for a given application [85].

The erosion–oxidation behavior of thermal sprayed Ni–Cr, Cr₃C₂–NiCr and stellite-6 coatings as a function of temperature and substrate materials under actual boiler conditions have been summarized [13]. Further, such data available in literature have been utilized to understand the variation in erosion–corrosion rate (mpy) as a function of temperature (°C) and coating deposition technique which is shown in Fig. 14. Irrespective of substrate material, the identically thick plasma sprayed Ni–20Cr coating with a bond coat of NiCrAlY performs slightly better up to 540 °C than the NiCrAlY coating may be noted. Further, the slightly thicker NiCrAlY coating alone perform better than Ni–20Cr top coating with NiCrAlY bond coat at ~ 750 °C temperature owing to the formation of well-adherent protective oxide scale by the “Y” content, which uniformly covers the coated surface [13]. Further, at ~ 750 °C in actual boiler environment, the plasma sprayed Stellite-6 coating outperforms both the plasma sprayed Ni–20Cr and NiCrAlY coatings.

However, detonation (D-Gun) sprayed or high velocity oxy-fuel (HVOF) sprayed Cr₃C₂–NiCr and Ni–20Cr coatings have 20 to 36 times higher erosion–corrosion resistance than the plasma sprayed Ni–Cr and stellite-6 coatings and retain their erosion–corrosion resistance properties up to 750 °C. Among the typical high velocity deposition

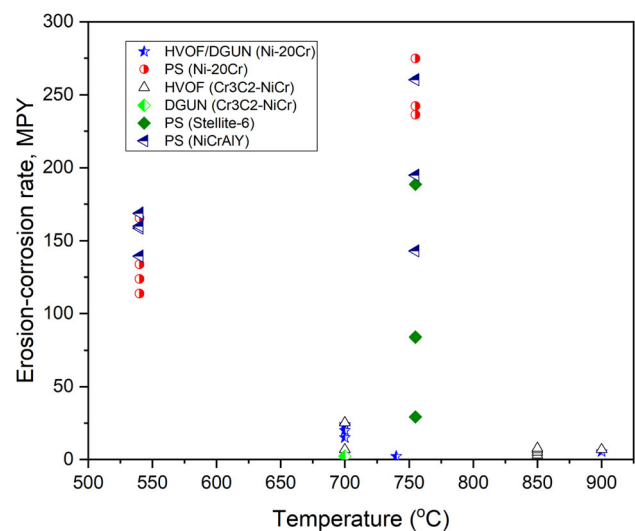


Fig. 14 E–C of various coatings in actual boiler conditions as a function of temperature and coating deposition technique. [13]

processes while spraying Cr₃C₂–NiCr on boiler steel substrate, the DSC sprayed Cr₃C₂–NiCr coating possess 3 times better erosion–corrosion resistance than HVOF sprayed coatings as shown in Fig. 15 [13]. Specific ability of DSC technology to retain the carbide phase without decomposition and to produce dense coatings as reported in several studies has been the prime reason behind such a better erosion–oxidation resistance than HVOF coatings [37, 40, 43].

It is to be noted that the thermal spray grade Cr₃C₂–NiCr powders are commercially available with varying NiCr proportions. Since Cr₃C₂ is a hard phase embedded in NiCr solid solution-based matrix phase, it will be interesting to understand the individual contributions of these two phases toward the overall erosion–oxidation resistance. In view of this, the erosion–oxidation rate of HVOF sprayed Cr₃C₂–

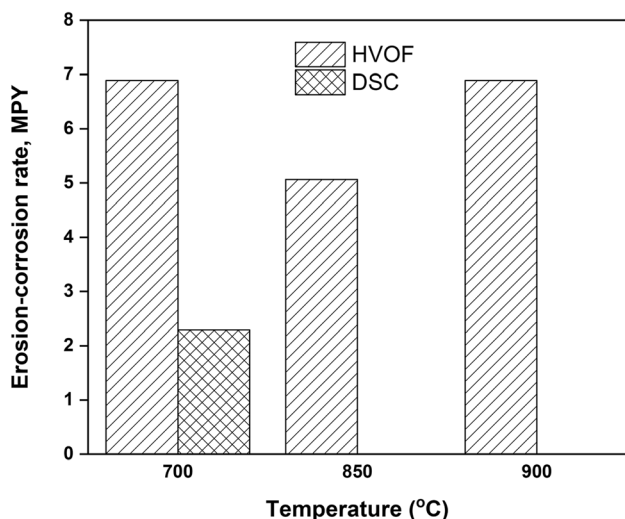


Fig. 15 E–C rate of Cr_3C_2 –NiCr coatings deposited by HVOF and detonation spray in actual boiler conditions [13]

NiCr coating deposited on T91 substrate as a function NiCr content/composition at 850 °C is illustrated in Fig. 16. Among all, the 65 Cr_3C_2 –35NiCr exhibits the lowest E–O rate due to the presence of compact, adherent, homogeneous and stable oxides of Ni and Cr with increasing NiCr content in the matrix. On the other hand, higher amounts of Cr_3C_2 phase proportion promotes the quicker crack growth through the weakly bonded oxidized regions and hence reduces the E–O resistance. [13, 88].

Overall, the best erosion–oxidation resistance of the thermal sprayed coatings significantly depends on the environment, temperature and impact velocity of erodent. At lower velocities and low temperatures, WC-based coatings will perform better under erosion–oxidation

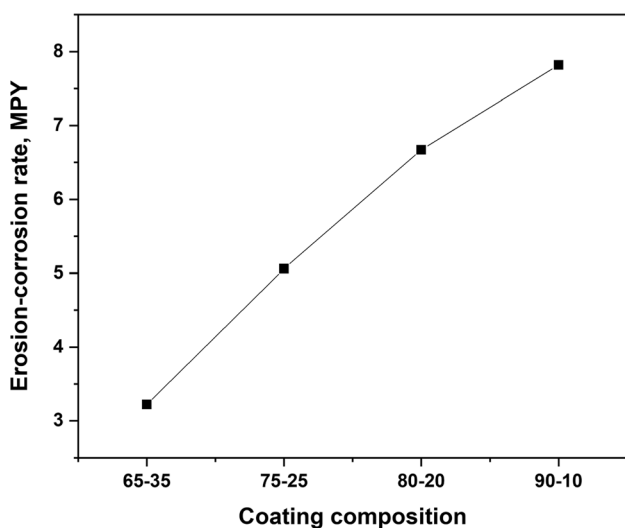


Fig. 16 E–C rate of Cr_3C_2 –NiCr coatings with varied NiCr content deposited by HVOF at 850 °C in actual boiler conditions. [13, 87]

conditions. On the other hand, with increasing temperature beyond 550 °C, Ni–Cr-based alloy coatings exhibit better performance than WC-based coatings up to 750 °C, while Cr_3C_2 -based coatings are preferred up to 850 °C [89–91]. Also, in general, the coatings deposited by high velocity processes such as HVOF and DSC exhibit better erosion–oxidation resistance than the plasma sprayed coatings. Formation of a thin, adherent and homogeneous protective oxide layer of Cr and Ni on the coated surface provides a condition to withstand E–O damage.

4.2.1 High-Temperature Erosion–Oxidation/Corrosion Prevention Methods

Based on the performance of various coatings under E–C/E–O conditions and associated coating removal mechanisms, one can believe that the coating hardness should be the simplest criterion to scale the E–C/E–O resistance. Yet, the relative carbide/metallic binder phase chemistry and its composition appear to be a more meaningful parameter to obtain E–C/E–O-resistant coatings. For instance, higher proportion of harder Cr_3C_2 content appears to promote easy pathways of cracking and therefore reduce the E–O resistance in Cr_3C_2 –NiCr coatings and an optimum NiCr content is required for better erosion–corrosion resistance of Cr_3C_2 -based coatings [13, 88]. Formation of η (complex) phases in WC–Co coatings can be hindered by adding TiC to WC–Co feedstock so as to enhance its erosion–oxidation resistance beyond 550 °C as well [92]. Hence, a careful selection of coating material and deposition technique is very essential to produce a microstructure that can significantly resist the E–C/E–O damage so that the components working under such harsh environments are protected in a better way.

Further, practical observation of the erosion–oxidation phenomenon has led to the formation of useful guidelines to enhance the erosion–oxidation performance of the material-based design criteria. These include reduction in the severity of erosive conditions by distribution of concentrated flow, reduction in the solid loading, shielding of the components from the erodent flow by replacing the pipe bends by T-junctions. A blocked tee arrangement has often been found to be very useful [9, 11, 13].

5 Summary and Future Work Scope

The vulnerability of materials to erosion–corrosion in severe environments demands surface solution to enhance the life of the components. Thermal spray techniques are widely employed to deposit various coatings to combat erosion and corrosion damages in aerospace and power industries. Owing to the high-temperature oxidation and

erosion resistance of advanced Cr_3C_2 and WC-based cermet coatings deposited either by HVOF or DSC/D-Gun techniques, these coatings have become the widely accepted solution in the power generation plants.

The E–C resistance of thermal spray coatings strongly depends on deposition technique, feedstock composition and the resulting coating's microstructure and phase constituents. Addition of Cr, Ni and Ti to the binder matrix enhances the E–C resistance of WC-based coatings due to the increase in noble nature as well as the ability to form a protective layer. In this regard, the WC–Co–Cr coatings are effective up to 550 °C as compared to WC–Co and WC–Ni coatings for E–C applications. Further, the addition of TiC and rare earth oxides to WC-based cermet feedstock results in a coating that exhibits better resistance even at higher operating temperature (> 550 °C). Beyond 550°, Cr_3C_2 –NiCr, Ni–Cr, NiCrAlY coatings become the candidate materials for E–O-resistant applications and the Cr_3C_2 –NiCr coatings are effective up to 850 °C. It is to be noted that the increasing NiCr content up to 35% in Cr_3C_2 –NiCr coatings has shown better properties in real boiler test conditions than the coatings with lower NiCr content.

Oxide coatings like Al_2O_3 , Al_2O_3 – TiO_2 and Cr_2O_3 – Al_2O_3 are also the candidate materials for both high-temperature E–O and ambient temperature E–C-resistant applications in alkaline environments. In addition, the E–C resistance of Ni-based and Fe-based intermetallic coatings has been explored recently. The Fe–Al intermetallic coatings are used up to 600 °C under high corrosion- and less wear-prone applications [93, 94]. Owing to the presence of Al in the Fe–Al coating, the aluminum oxide formed is found to protect the component surface from oxidative erosion. Further, the Fe–Al coatings are relatively a cost effective solution to replace the expensive Ni/Co binders in WC-based coatings as well as direct replacement of WC-based and Ni-based coatings for specific applications [93, 94].

Owing to the presence of various defects such as porosity, inter-splat boundaries, un-melted particles and undesirable phases in the thermal spray coatings, the post-coating treatments such as sealing of pores, laser melting and heat treatment have been reported to yield positive benefits by way of improved erosion–corrosion resistance by protecting the coating from ingress of solution and gaseous species through defective regions [72–76].

Although the erosion–corrosion behavior of WC-based cermet coatings at ambient temperature is extensively reported, only a few studies are reported so far to understand the E–C performance and material removal mechanism of Cr_3C_2 -based coatings. Even though there are studies on the E–C behavior of thermal sprayed coatings, they are system specific and cannot be extended to compare the same with the results of other coating material deposition technique combinations. For example, erosion–

corrosion behavior of WC–Co–Cr coatings is widely studied in NaCl solution. However, the knowledge acquired in the case of WC–Co–Cr coatings cannot be directly translated to WC–Co coatings.

In spite of employing the identical deposition technique, such a translation of knowledge becomes difficult because of varying feedstock morphologies and particle size ranges that alter the final coating microstructure including the porosity and phase composition. In this regard, there exists a significant research scope where the E–C maps and material removal mechanisms of various thermal sprayed coating need out-and-out investigation which helps in assessing the overall performance. The mapping based on various parameters and their ranges to understand the material loss mechanisms need to be standardized. In particular, the maps generated by mean surface roughness of coating may often be misleading [85–87]. In addition, since the erosion–corrosion behavior of coatings is quite complex and therefore demands an extensive modeling coupled with experimental studies to comprehensively understand the material loss, the suitable coating choice for particular application becomes identifiable [95]. Last but not least, a standard test system needs to be developed to study the influence of all the test parameters at once in a combined erosion–corrosion test rig.

There is a constant demand from the industry to find cost effective solutions to design the components suitable to work under harsher environments. In addition to the available carbide coatings, Ni–Cr and oxide coatings have been explored for various wear and corrosion resistance applications; the recent developments have also shown that the Fe-based amorphous coating appears to be a candidate material for E–C-resistant applications, especially at ambient temperatures [78]. More alloy compositions are yet to be explored, and futuristic studies will be focused to use them as protective coating alternatives for E–O resistant application. For instance, oxide dispersion strengthened alloys of suitable chemistry may also serve as the candidate coatings for erosion–oxidation resistance applications [9]. Oxide-dispersed Fe-based and Ni-based coatings as well as intermetallic coatings demonstrate a promise to replace the expensive coatings on various industrial components subjected to erosion–corrosion.

With the advent of high velocity air fuel (HVOF) and axially fed plasma spray systems now commercially available with a promise to deliver coatings with significantly reduced cost and improved deposition rates and efficiencies, these techniques are yet to be fully explored for depositing erosion–corrosion/oxidation resistant coatings on industry scale.

Acknowledgements The authors would like to thank Ms. D. Vijaya Lakshmi, Centre for Engineered Coatings for assisting us with the

literature on “high temperature erosion–oxidation behavior of thermal sprayed coatings.”

References

- Wellman R G, and Nicholls J R, *Wear* **256** (2004) 907.
- Stack M M, and Abd El Badia T M, *Surf Coat Technol* **201** (2006) 1335.
- Mehta J, Mittal V K, and Gupta P, *J Appl Sci Eng* **20** (2017) 445.
- Tribocorrosion of passive metals and coatings, (eds) Dieter L, and Stefano M, *A Volume in Woodhead Publishing Series in Metals and Surface Engineering* (2011) ISBN: 978-1-84569-966-6.
- Yoganandh J, Natarajan S, and Babu S P K, *Trans IIM* **66** (2013) 437.
- Prozhega M V, Tatus N A, Samsonov S V, Kolyuzhni O Y, and Smirnov N N, *J Frict Wear* **35** (2014) 155.
- Wood R J K, Herd S, and Thakare M R, *Tribol Int* **119** (2018) 491.
- El Rayes M M, Abdo H S, and Khalil K A, *Int J Electrochem Sci* **8** (2013) 1117.
- Wright I G, Is there any reason to continue research efforts in erosion–corrosion? in *Proc John Stringer Symposium on High Temperature Corrosion, 2001*, (eds) Tortorelli P F, Wright I G, and Hou P V, ASM International, Ohio (2003), p. 107.
- Thomas C B B, and Wood R J K, *J Bio Tribo Corros* **3** (2017) 14.
- Szymanski K, Hernas A, Moskal G, and Myalska H, *Surf Coat Technol* **268** (2015) 153.
- Wang B Q, *Wear* **188** (1995) 40.
- Kumar S, Kumar M, Handa A, *Eng Fail Anal* **94** (2018) 379.
- Wang B Q, *Wear* **199** (1996) 24.
- Singh H, Chatha S S, Sidhu H S, and Sharma K, *Int J Adv Mechatron Robot* **3** (2011) 85.
- Wozniowski A, *Surf Coat Technol* **43–44** (1990) 848.
- Al-Hamed A, Fadhli H Y, Al-Mutairi S, Yilbas B S, Hashmi M S J, and Stokes J, *WIT Trans Eng Sci Surf Effects Contact Mech XI* **78** (2013) 215.
- Wood R J K, *J Phys D Appl Phys* **40** (2007) 5502.
- Tiwari A, Seman S, Singh G, Jayaganthan R, *Coatings* **9** (2019) 400.
- Keshavamurthy R, Naveena B E, Sekhar N, in *Production, Properties and Applications of High Temperature Coatings. ACME Book Series*, (eds) Pakseresht A H, IGI Global, Hershey (2018), p. 246.
- Davis J R, *Handbook of Thermal Spray Technology*, ASM International, Materials Park, Ohio (2004).
- Fauchais P L, Heberlein J V R, and Boulos M, *Thermal Spray Fundamentals*, Springer, New York (2014).
- Powlowski L, *The Science and Engineering of Thermal Spray Coatings* (2008) ISBN: 9780471490494.
- Espallargas N, *Future Development of Thermal Spray Coatings* (2015) ISBN: 978-0-85709-769-9.
- Champagne V K, *The Cold Spray Materials Deposition Process* (2007) ISBN: 9781845691813/9781845693787.
- Papyrin A, *Cold Spray Technology* (2006) ISBN: 9780080451558/9780080465487.
- Sanpo N, *Solution Precursor Plasma Spray System* (2014) ISBN: 978-3-319-07025-4.
- Fauchais P, Rat V, Coudert J F, Salas R E, and Montavon G, *Surf Coat Technol* **202** (2008) 4309.
- Tarasi F, Medraj M, Dolatabadi A, Berghaus J O, and Moreau C, *J Therm Spray Technol* **17** (2008) 685.
- Siegmann S, and Abert C, *Surf Coat Technol* **220** (2013) 3.
- Wood R J K, *Int J Refract Met Hard Mater* **28** (2010) 82.
- Verdon C, Karimi A, and Martin J L, *Mater Sci Eng A* **234–236** (1997) 731.
- Sadeghi E, Markocsan N, and Joshi S V, *J Therm Spray Technol* **28** (2019) 1749.
- Sadeghi E, Markocsan N, and Joshi S V, *J Therm Spray Technol* **28** (2019) 1789.
- Matikainen V, Koivuluoto H, and Vuoristo P, *Wear* **446–447** (2020) 203188.
- Rao D S, Kumar G S, Sen D, and Joshi S V, in *Thermal Sprayed Coatings and Their Tribological Performances, Chapter 10*, (eds) Roy M, Devim J, IGI Global, Hershey (2015), 294.
- Babu P S, Basu B, and Sundararajan G, *Acta Mater* **56** (2008) 5012.
- Babu P S, Sen D, Jyothirmayi A, Krishna L R, and Rao D S, *Ceram Int* **44** (2018) 2351.
- Ulianitsky V, Shtertser A, Zlobin S, and Smurov I, *J Therm Spray Technol* **20** (2011) 791.
- Sundararajan G, and Babu P S, *Trans IIM* **62** (2009) 95.
- Sundararajan G, Sivakumar G, Sen D, Rao D S, and Ravichandra G, *Int J Refract Met Hard Mater* **28** (2010) 71.
- Somaraju K R C, Rao D S, Sivakumar G, Sen D, Rao G V N, and Sundararajan G, in *Proceedings of 2nd International Thermal Spray Conference (ITSC)*, (eds) Berndt C C (2000), p. 309.
- Babu P S, Rao D S, Rao G V N, and Sundararajan G, *J Therm Spray Technol* **16** (2007) 281.
- Sen D, Chavan N M, Rao D S, and Sundararajan G, *J Therm Spray Technol* **19** (2010) 805.
- Babu P S, Madhavi Y, Krishna L R, Rao D S, and Padmanabham G, *JOM* **70** (2018) 2636.
- Zu J B, Hutchings I M, and Burstein G T, *Wear* **140** (1990) 331.
- ASTM G 119, *Standard Guide for Determining Synergism Between Wear and Corrosion*, **2009** (2016).
- Watson S W, *Wear* **181** (1995) 476.
- Schorr M, Weintraub E, and Andrasi D, *Erosion–Corrosion Measuring Devices* (1989) p. 151.
- Rajahram S S, Harvey T J, and Wood R J K, *Wear* **267** (2009) 244.
- Singh H, Kaur M, and Prakash S, *J Therm Spray Technol* **25** (2016) 1192.
- Antonov M, Veinthal R, Saarivirta E H, Hussainova I, Vallikivi A, Lelis M, and Priss J, *Tribol Int* **68** (2013) 35.
- Kaushal G, Singh H, and Prakash S, *Metall Mater Trans A* **42** (2011) 1836.
- Wang B Q, and Luer K, *Wear* **174** (1994) 177.
- Wang B Q, and Geng G Q, *Surf Coat Technol* **43–44** (1990) 859.
- Stack M M, Stott F H, and Wood G C, *J Phys IV* **3** (1993) 687.
- Souza V A D, and Neville A, *Wear* **255** (2003) 146.
- Souza V A D, and Neville A, *Wear* **259** (2005) 171.
- Berget J, Rogne T, and Bardal E, *Surf Coat Technol* **201** (2007) 7619.
- Espallargas N, Berget J, Guilemany J M, Benedetti A V, and Suegama P H, *Surf Coat Technol* **202** (2008) 1405.
- Saha G C, Khan T I, and Zhang G A, *Corros Sci* **53** (2011) 2106.
- Berget J, Bardal E, Rogne T, in *Proceedings of the 15th International Thermal Spray Conference* (1998), p. 305.
- Hong S, Wu Y, Gao W, Zhang J, Zheng Y, and Zheng Y, *Int J Refract Met Hard Mater* **74** (2018) 7.
- Toma D, Brandl W, and Marginean G, *Surf Coat Technol* **138** (2001) 149.
- Liu Y, Hang Z, Xi N, Chen H, Ma C, and Wu X, *Appl Surf Sci* **431** (2018) 55.
- Tan K S, Wharton J A, and Wood R J K, *Wear* **258** (2005) 629.
- Stack M M, and Abd El Badia T M, *Wear* **261** (2006) 1181.
- Stack M M, and Abd El Badia T M, *Wear* **264** (2008) 826.
- Farokhzadeh K, Fillion R M, and Edrissy A, *J Mater Eng Perform* **28** (2019) 7419.

70. Souza V A D, Neville A, *Wear* **263** (2007) 339.
71. Hong S, Wu Y, Zhang J, Zheng Y, Qin Y, Gao W, and Li G, *Trans IIM* **68** (2015) 151.
72. Janette B, Anna G, Dagmar D, and Jozef B, *Mater Sci Forum* **811** (2015) 63.
73. Shrestha S, Hodgkiess T, and Neville A, *Wear* **259** (2005) 208.
74. Zhang S H, Cho T Y, Yoon J H, Li M X, Shum P W, Kwon S C, *Mater Sci Eng B* **162** (2009) 127.
75. Mohan Reddy K R R, Ramanaiah N, and Sarcar M M M, *J King Saud Univ—Eng Sci* **29** (2017) 84.
76. Armada S, Tilset B G, Pilz M, Liltvedt R, Bratland H, and Espallargas N, *J Therm Spray Technol* **20** (2011) 918.
77. Peat T, Galloway A M, Toumpis A I, and Harvey D, *Surf Coat Technol* **299** (2016) 37.
78. Liu X Q, Zheng Y G, Chang X C, Hou W L, and Wang J Q, *Mater Sci Forum* **633–634** (2010) 685.
79. Kawahara Y, *J Therm Spray Technol* **16** (2007) 202.
80. Kablov E N, and Muboyadzhyan S A, *Russ Metall* **6** (2017) 494.
81. Kaur M, Singh H, and Prakash S, *Anti-Corros Methods Mater* **55** (2008) 86.
82. Kaur M, Singh H, and Prakash S, *Adv Mater Res* **26–28** (2007) 1345.
83. Saladi S, Menghani J, and Prakash S, *Trans IIM* **67** (2014) 623.
84. Kuniوشي C T, Correa O V, and Ramanathan L V, *Surf Eng* **22** (2006) 121.
85. Kuniوشي C T, Correa O V, and Ramanathan L V, *Mater Sci Forum* **530–531** (2006) 117.
86. Kuniوشي C T, Correa O V, and Ramanathan L V, *Mater Res* **8** (2005) 125.
87. Da Cunha C A, Correa O V, Sayeg I J, and Ramanathan L V, *Mater Res* **20** (2017) 994.
88. Bhatia R, Sidhu H S, and Sidhu B S, *Metal Mater Trans E* **2** (2015) 1011.
89. Mishra S B, and Prakash S, *Surf Eng* **31** (2015) 29.
90. Matthews S, James B, and Hyland M, *Corr Sci* **50** (2008) 3087.
91. Mishra S B, Chandra K, and Prakash S, *Surf Coat Technol* **216** (2013) 23.
92. Myalska H, Lusvarghi L, Bolelli G, Sassatelli P, and Moskal G, *Surf Coat Technol* **371** (2019) 401.
93. Senderowski C, Bojar Z, Wolczynski W, and Powlowski A, *Intermetallics* **18** (2010) 1405.
94. Cinca N, Cygan S, Senderowski C, Jaworska L, Dosta S, Cano I G, and Guilemany J M, *Coatings* **8** (2018) 268.
95. Stack M M, and Bray L, *Wear* **186–187** (1995) 273.

Publisher's Note Springer Nature remains neutral with regard to jurisdictional claims in published maps and institutional affiliations.